Linear and nonlinear verification of gyrokinetic microstability codes

R. V. Bravenec, J. Candy, M. Barnes, and C. Holland

Citation: Phys. Plasmas **18**, 122505 (2011); doi: 10.1063/1.3671907
View online: http://dx.doi.org/10.1063/1.3671907
View Table of Contents: http://pop.aip.org/resource/1/PHPAEN/v18/i12
Published by the American Institute of Physics.

Linear and nonlinear verification of gyrokinetic microstability codes

R. V. Bravenec,[1,a)] J. Candy,[2] M. Barnes,[3,4,b)] and C. Holland[5]
[1]*Fourth State Research, 503 Lockhart Dr., Austin, Texas 78704-4335, USA*
[2]*General Atomics, P.O. Box 85608, San Diego, California 92186-5608, USA*
[3]*Rudolf Peierls Centre for Theoretical Physics, University of Oxford, Oxford OX1 3NP, United Kingdom*
[4]*EURATOM/CCFE Fusion Association, Culham Science Centre, Abingdon OX14 3DB, United Kingdom*
[5]*University of California at San Diego, San Diego, California 92093-0417, USA*

(Received 28 June 2011; accepted 25 October 2011; published online 30 December 2011)

Verification of nonlinear microstability codes is a necessary step before comparisons or predictions of turbulent transport in toroidal devices can be justified. By verification we mean demonstrating that a code correctly solves the mathematical model upon which it is based. Some degree of verification can be accomplished indirectly from analytical instability threshold conditions, nonlinear saturation estimates, etc., for relatively simple plasmas. However, verification for experimentally relevant plasma conditions and physics is beyond the realm of analytical treatment and must rely on code-to-code comparisons, i.e., benchmarking. The premise is that the codes are verified for a given problem or set of parameters if they all agree within a specified tolerance. True verification requires comparisons for a number of plasma conditions, e.g., different devices, discharges, times, and radii. Running the codes and keeping track of linear and nonlinear inputs and results for all conditions could be prohibitive unless there was some degree of automation. We have written software to do just this and have formulated a metric for assessing agreement of nonlinear simulations. We present comparisons, both linear and nonlinear, between the gyrokinetic codes GYRO [J. Candy and R. E. Waltz, J. Comput. Phys. **186**, 545 (2003)] and GS2 [W. Dorland, F. Jenko, M. Kotschenreuther, and B. N. Rogers, Phys. Rev. Lett. **85**, 5579 (2000)]. We do so at the mid-radius for the same discharge as in earlier work [C. Holland, A. E. White, G. R. McKee, M. W. Shafer, J. Candy, R. E. Waltz, L. Schmitz, and G. R. Tynan, Phys. Plasmas **16**, 052301 (2009)]. The comparisons include electromagnetic fluctuations, passing and trapped electrons, plasma shaping, one kinetic impurity, and finite Debye-length effects. Results neglecting and including electron collisions (Lorentz model) are presented. We find that the linear frequencies with or without collisions agree well between codes, as do the time averages of the nonlinear fluxes without collisions. With collisions, the differences between the time-averaged fluxes are larger than the uncertainties defined as the oscillations of the fluxes, with the GS2 fluxes consistently larger (or more positive) than those from GYRO. However, the electrostatic fluxes are much smaller than those without collisions (the electromagnetic energy flux is negligible in both cases). In fact, except for the electron energy fluxes, the absolute magnitudes of the differences in fluxes with collisions are the same or smaller than those without. None of the fluxes exhibit large absolute differences between codes. Beyond these results, the specific linear and nonlinear benchmarks proposed here, as well as the underlying methodology, provide the basis for a wide variety of future verification efforts.
 [doi:10.1063/1.3671907]

I. INTRODUCTION

The state of the art in plasma microstability theory is represented by complex nonlinear gyrokinetic codes, which run on massively parallel supercomputers. Some of the U.S. codes (GYRO,[1] GS2,[2] GEM,[3] PG3EQ,[4] and GTC[5]) are now able to compute the saturated fluctuations in not only the electrostatic potential but also fluctuations in the electromagnetic potentials and in the densities and temperatures of multiple plasma species. The codes include kinetic electrons (passing and trapped) and gyrokinetic impurities with interspecies collisions. Plasma shaping is modeled via the Miller formalism[6,7] and/or actual numerical equilibria, e.g., from EFIT.[8] Equilibrium $\mathbf{E} \times \mathbf{B}$ flow shear—important for turbulence stabilization[9] and crucial for realistic nonlinear simulations in rapidly rotating plasmas—is functional in all the above codes. Therefore, these codes have the capability of computing the turbulence-induced particle and energy fluxes thought to dominate transport in actual experiments. Nonlinear simulations are now being applied to predict performance in ITER (Ref. 10), while linear application of the codes has become routine for interpreting experimental transport results.

Gyrokinetic codes have demonstrated the capability of predicting particle fluxes and electron/ion energy fluxes in agreement with power balance analysis and fluctuation characteristics in agreement with experimental measurements.[11–20] However, robust agreement of all aspects of gyrokinetic simulation results with experimental measurements ("validation") has not been consistently found in studies to date. More

[a)]Electronic mail: rvbravenec@4th-state.com.
[b)]Present address: Plasma Science and Fusion Center, MIT, Cambridge, Massachusetts 02139, USA

fundamentally, the codes have not demonstrated that they correctly solve the equations upon which they are based ("verification"), particularly when nonlinear dynamics are considered. The code developers have performed their own individual nonlinear verification exercises, but they have had to do so indirectly by comparing their predictions with analytical instability threshold conditions, nonlinear saturation estimates, etc. Verification for more realistic plasma conditions must, therefore, rely on comparisons among codes ("benchmarking"), the idea being that the underlying equations are being solved correctly if all the codes agree. Of course, the definition of "agree" must be quantified, because the codes never can be expected to perfectly agree. This topic we address later in this work. Note that this idea presumes that the codes in question are all intending to solve the exact same formulation of the equations, which is not always the case, e.g., with respect to terms like the so-called parallel nonlinearity.[21]

Cross-code verification exercises require clearly defined common benchmark cases, specifying both the code inputs and quantities to be compared. In the past, the developers engaged in formal comparisons—the "Numerical Tokamak,"[22] The Cyclone Project,[23] and the Plasma Microturbulence Project—in which computations of thermal diffusivities were compared among codes for a limited set of simple plasma profiles. These comparisons ignored magnetic fluctuations, collisions, trapped electrons, impurities, plasma shaping, and equilibrium $\mathbf{E}\times\mathbf{B}$ flow shear, i.e., they were of limited relevance to experiments. Because GYRO, GS2, and GEM have become much more powerful, the Center for the Study of Plasma Microturbulence (CSPM)[24] was established in order for a group of developers and users to collaborate on issues such as verification and validation ("V&V"). Similarly, the Gyrokinetic Particle Simulation for Turbulent Transport in Burning Plasmas,[25] concentrating on applications of the GTC code, was formed.

Verification and validation have been of general interest throughout the computational physics community for some time.[26] In fact, V&V components are required of all recent grant applications to the U. S. Department of Energy Fusion Energy Sciences program. Furthermore, the editorial board of Physics of Plasmas has endorsed such efforts for physics understanding.[27] As a consequence, V&V of microstability codes has emerged as a major research topic in the tokamak transport community. Verification and validation of the major nonlinear gyrokinetic codes also would be a necessary step in the Fusion Simulation Project (FSP),[28] whose goal is to provide a predictive capability for operation of ITER and next-step devices.

Although verification is a logical predecessor to validation, more attention has been placed on the latter. It should be stressed that validation does not supersede verification. A validated code is not necessarily verified. This is because true validation requires assessing the model prediction uncertainties, for instance propagating uncertainties in input parameters such as equilibrium profiles and gradients. Regardless of the outcome of this exercise, there is no way to distinguish between code errors and experimental uncertainties without verification of the codes for the problem in question.

The goal of this work is to verify the linear and nonlinear predictions of the continuum (Eulerian) δf gyrokinetic microstability codes GYRO and GS2 for experimentally relevant parameters and physics, thereby formulating meaningful benchmarks through "apples-to-apples" comparisons between them. Apples-to-apples here means not only using the same plasma conditions but also including the same physics and having sufficient temporal, spatial, and velocity-space resolutions. Comparisons are restricted to GYRO and GS2 because of the authors' experience and the codes' extensive documentation that allow use by the general community. They both employ a fixed grid (Eulerian) in five-dimensional phase space. Thus, they are immune from noise related to sampling error, which can accumulate during a Lagrangian particle-in-cell (PIC) computation[29] if not controlled.[30] Instead, the Eulerian codes control the build-up of entropy on small scales by use of physical collisions and well-known numerical dissipation techniques, which have been shown to have no impact on the large-scale physics of interest for many cases.[31]

The GS2 code was the first to be developed. It is a nonlinear generalization of the gyrokinetic stability code GSTOTAL,[32] which employed an implicit initial-value algorithm in the ballooning ("flux-tube") limit. As such, it assumes mean plasma parameters do not change over the simulation domain. GS2 was the first nonlinear gyrokinetic code to include the crucial nonadiabatic electron dynamics required for trapped-electron modes and electromagnetic physics. Nonuniform coordinate meshes are used in velocity space to improve the resolution, particularly for the trapped-passing boundary.[33] An operator-splitting scheme is used, so that the linear terms may be treated implicitly. The nonlinear terms are evaluated with a de-aliased pseudo-spectral algorithm in the plane perpendicular to the field line. A third-order Adams–Bashforth scheme is used to advance the nonlinear terms in time. A small amount of upwind diffusion is typically used, only in the direction along the field line. Good parallel performance is achieved by employing multiple-domain decomposition in four of the five dimensions at all times. The Bessel functions appearing in the expressions for the fluctuating quantities (which represent the gyro-averages) are evaluated in Fourier space. This guarantees the applicability of the algorithms to arbitrary perpendicular length scales. The code employs a velocity-space collision operator.[34,35]

Development of GYRO started in 1999. The primary goal was to generalize GS2 by retaining profile-variation effects to allow, in principle, deviations from pure gyro-Bohm scaling ("global" simulations). The numerical methods for GYRO were initially patterned after GS2 wherever possible, although there was no sharing of code. In the end, many significant departures from GS2 were required to meet the GYRO design target and to simultaneously increase computational efficiency. By 2001, GYRO had the ability to operate either globally using Dirichlet (zero-value) radial boundary conditions or locally using flux-tube (periodic) boundary conditions. An implicit-explicit Runge-Kutta (IMEX-RK) integrator was eventually added to overcome the electrostatic Alfven–wave Courant limit, which can severely limit the time step for large-domain simulations. Independently, a novel poloidal discretization scheme solved the Ampere cancellation

problem. Magnetic fluctuations are treated the same as in GS2, e.g., the curvature is not set equal to the ∇B drift.

To enforce the apples-to-apples requirement, all the code comparisons were performed in the flux-tube (local) limit, which is equivalent to assuming $\rho^* = \rho_s/a$ is vanishingly small, where ρ_s is the ion-sound gyroradius and a is the plasma minor radius. (These parameters will be defined more precisely in Sec. III.) Plasma shape was treated to high accuracy using the local equilibrium method with Miller shape parameterization.[6,7] All computations included three kinetic species: electrons, deuterium, and one impurity (C^{6+}). The simulations retained finite β (the ratio of plasma pressure to magnetic-field pressure) and transverse magnetic fluctuations. Compressional fluctuations were ignored because of the small value of β in the discharge analyzed here. A guiding-center Lorentz collision operator was used for electron collisions. This operator is solved with an implicit discretization in both GYRO and GS2. The Debye-length effect in the Poisson equation was retained in the linear computations, which were conducted over a wide range of poloidal wave number k_θ. The electrons were fully gyrokinetic except electron gyro-averaging was ignored for $k_\theta \rho_s < 1$ in GYRO. Nonlinear comparisons were restricted to low k_θ in order to minimize the simulation cost, and because experiments and previous simulations have shown the turbulence to be dominated by low-k_θ fluctuations for the conditions considered. Plasma rotation and rotation shear effects were neglected for simplicity. We refer to the model that includes transverse magnetic fluctuations, accurate plasma shape, three kinetic species, and electron collisions as "full physics" in the following.

II. VERIFICATION PROCEDURE

The comparison procedure is as follows:

1. A single routine is used to extract plasma parameters from ONETWO (Ref. 36) or TRANSP (Ref. 37) analysis and to write to a file of a particular format.
2. A linear input file is generated for GYRO and then translated into an input file for GS2 by another routine. (This eliminates potential errors introduced by separate data readers.)
3. The codes are run with all the physics features listed earlier.
4. If differences are found between codes, then collisions, magnetic fluctuations, etc., are removed one at a time until agreement is reached ⇒ "reduced" benchmark.
5. Physics features are reintroduced one at a time in different order:
   a. agreement ⇒ successively more complex benchmarks and
   b. disagreement ⇒ source(s) of problem, e.g., collisions or combination of impurities and trapped electrons.
6. Results are presented to code developers who must concur with findings, then help seek resolution.
7. Steps 5 and 6 are repeated until all terms are included ⇒ full physics benchmark.
8. Nonlinear GS2, GYRO input files are generated and steps 3–7 are repeated.
9. Entire procedure is repeated for different radii, discharge times, discharge numbers, and devices.

There are potential pitfalls in step 2 because of differences in normalizations and definitions of some GYRO and GS2 input parameters. For the benefit of others who may be running both codes, we present these in the Appendix.

This procedure requires keeping track of the linear and nonlinear inputs and results for each physics model at multiple times, radii, discharges, and devices. Likewise, comparisons of the code results for each condition must be organized. This could be prohibitive unless there was some degree of automation. As a consequence, a number of Python utilities have been written to automate much of the work.

III. COMPARISONS BETWEEN GYRO AND GS2

The DIII-D discharge 128913 was analyzed 1.5 s into the discharge at the radius $\rho = 0.5$, where ρ is the square root of the toroidal flux normalized to that at the outermost closed flux surface. Local parameters are listed in Table I, where r is the half-width of the flux surface at the elevation of the centroid, a is the value of r at the outermost flux surface, and $\rho^* = \rho_s/a$. Here $\rho_s \equiv c_s/\omega_{ci}$, where $c_s \equiv (kT_e/m_i)^{1/2}$, $\omega_{ci} \equiv eB_0/m_i c$, m_i is the mass of the main ion (D), and B_0 is the magnetic field at R_0, the center of the flux surface. The other parameters have the conventional definitions and are defined in the table. Further details of the discharge can be found in Refs. 13 and 17.

Following the steps outlined earlier, we first perform linear analysis. We set $k_r \rho_s = 0$ in GS2, where k_r is the radial wave number, which yields the fastest growing mode for each value of k_θ. Because GYRO treats the radial dimension in configuration space rather than wave-number space, it is not necessary to choose discrete radial wave numbers.

TABLE I. Parameters of DIII-D discharge 128913 at 1.5 s and $\rho = 0.5$ ($r = 0.33$ m, $a = 0.60$ m).

n_e (10^{19} m^{-3})	2.11
T_e (keV)	0.992
n_i/n_e	0.935
n_{imp}/n_e	0.011
$T_i/T_e = T_{inp}/T_e$	0.828
$a/L_{ne} = a\ \mathrm{dln}(n_e)/\mathrm{d}r$	1.07
$a/L_{ni} = a\ \mathrm{dln}(n_i)/\mathrm{d}r$	1.10
$a/L_{Te} = a\ \mathrm{dln}(T_e)/\mathrm{d}r$	2.64
$a/L_{Ti} = a\ \mathrm{dln}(T_i)/\mathrm{d}r$	1.81
$a/L_{Timp} = a\ \mathrm{dln}(T_{imp})/\mathrm{d}r$	1.81
$R_0(r)/a$	2.81
$\Delta = \mathrm{d}R_0(r)/\mathrm{d}r$	−0.0855
q	1.805
$s = r\ \mathrm{dln}(q)/\mathrm{d}r$	0.580
κ	1.30
$s_\kappa = r\ \mathrm{dln}(\kappa)/\mathrm{d}r$	0.0457
δ	0.150
$s_\delta = r\ \mathrm{d}\delta/\mathrm{d}r$	0.174
β	0.00346
ρ^*	0.00366
Z_{eff}	1.32
$\nu_{ei}\ a/c_s$	0.112

The real and imaginary frequencies for full physics are shown in Fig. 1. The time steps and numbers of velocity-space grid points (trapped and passing pitch angles and energy) were chosen to achieve convergence of each code. Below $k_\theta\rho_s \sim 1$, the modes propagate in the ion diamagnetic (negative) direction, suggesting that they are ion-temperature-gradient (ITG) modes. The magnitudes of the growth rates below $k_\theta\rho_s \sim 0.6$ increase with $k_\theta\rho_s$ and then decrease toward a minimum at $k_\theta\rho_s \sim 1.5$ where the propagation direction changes sign. The modes propagate in the electron diamagnetic (positive) direction for $k_\theta\rho_s \geq 1$, indicating that they are trapped-electron modes (TEMs) at the lowest $k_\theta\rho_s$ in this range, electron-temperature-gradient (ETG) modes at the highest $k_\theta\rho_s$, and a combination in between. The growth rates increase roughly linearly with $k_\theta\rho_s$ until $k_\theta\rho_s \approx 24$ ($k_\theta\rho_e \approx 0.4$) where they peak and then rapidly vanish.

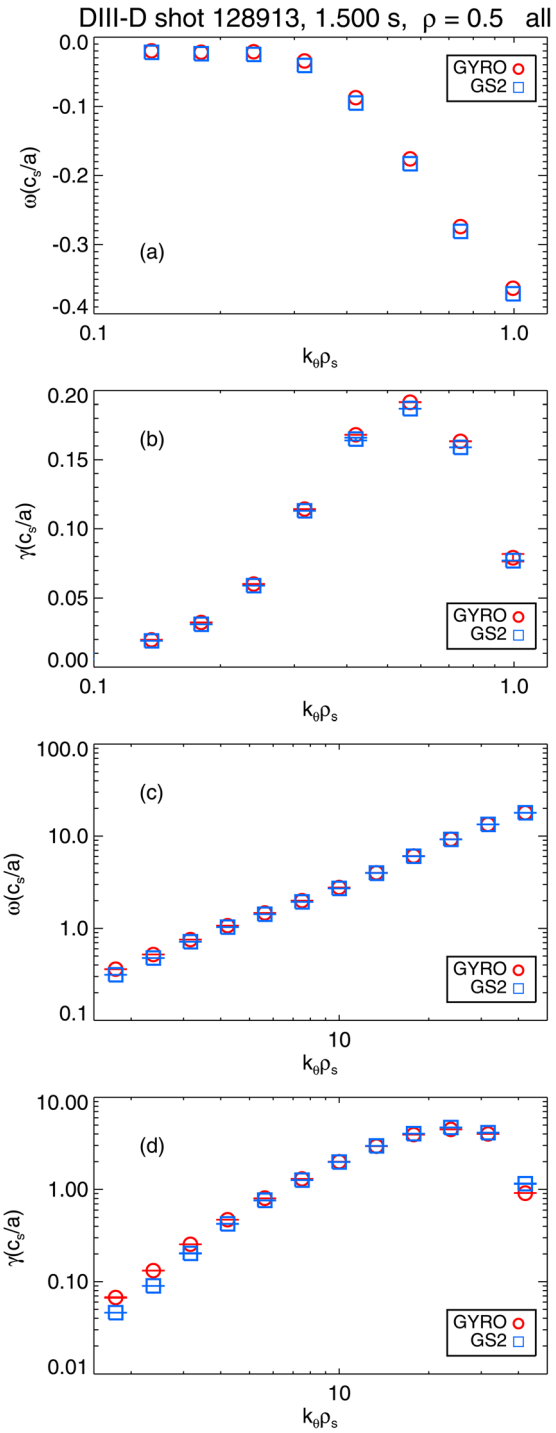

FIG. 1. (Color online) GYRO and GS2 frequencies for full-physics model (electromagnetic; kinetic electrons, main ions, and one impurity; shaping; electron collisions) at $\rho = 0.5$. (a) Real frequencies and (b) growth rates for $0.1 \leq k_\theta\rho_s \leq 1.2$. (c) Real frequencies and (d) growth rates for $1.5 \leq k_\theta\rho_s \leq 50$. Negative (positive) real frequencies indicate propagation in the ion (electron) diamagnetic direction.

Agreement between GYRO and GS2 is excellent except for the growth rates in the range $1.5 \leq k_\theta\rho_s \leq 4$. This region is where TEMs are active, as verified by assuming adiabatic electrons, when the growth rates are found to vanish.

Following the procedure outlined in Sec. II, we remove a physics feature and repeat. Since TEMs are sensitive to collisions, we remove those first. The results are shown in Fig. 2. The agreement between codes is much better in the TEM region, implying the slight discrepancies in Fig. 1 are due to small differences in collision operators. We have removed impurities, shaping, and magnetic fluctuations individually only to find that the discrepancies with collisions remain (although smaller). Note that below $k_\theta\rho_s \sim 0.5$, the modes propagate in the electron diamagnetic direction. It is possible that the modes here are hybrids, best described as "electron-direction" modes. Note also that in the region $k_\theta\rho_s \sim 0.2$, the growth rates are much larger without collisions.

Although we have shown excellent linear agreement between codes with and without collisions and including transverse magnetic fluctuations, plasma shaping, kinetic electrons, and one kinetic impurity, we have not done so for each of the above physics components individually. As we will show in the following nonlinear results, the contribution of magnetic fluctuations is small, so ignoring these would not contribute much to the code comparisons. For self-consistency, modifying the plasma shape is not as simple as changing the Miller parameters while leaving all the other plasma parameters the same. A proper code comparison for a different plasma shape would require a different discharge. Therefore, in this work, we are left with examining code agreement for adiabatic electrons or neglecting the impurity.

Shown in Fig. 3 are the real and imaginary frequencies assuming adiabatic electrons. Frequencies above $k_\theta\rho_s \sim 1$ are not shown because the modes are all stable. We observe excellent agreement between the codes except for the growth rate at $k_\theta\rho_s \sim 1$. However, the growth rate rapidly vanishes here. These results indicate it is unlikely that code errors involving one physics component could compensate for those in another.

We next turn to nonlinear simulations, which used 16 poloidal modes spanning the range $0 \leq k_\theta\rho_s \leq 1$. The simulation box was the same for both codes: The normalized poloidal box size $L_\theta/\rho_s \approx 100$ was simply the normalized wavelength of the smallest nonzero value of $k_\theta\rho_s$. The normalized radial box size was $L_r/\rho_s \approx 150$ and the number of radial grid points was 144 for GS2 and a third greater[38] for GYRO (192). Thus, the grid spacing was $\Delta r/\rho_s \approx 1$ and 0.8, respectively. Fluxes are normalized to the gyro-Bohm electron energy flux $Q_{GB} = n_e T_e c_s (\rho_s/a)^2$ or particle flux $\Gamma_{GB} = Q_{GB}/T_e$.

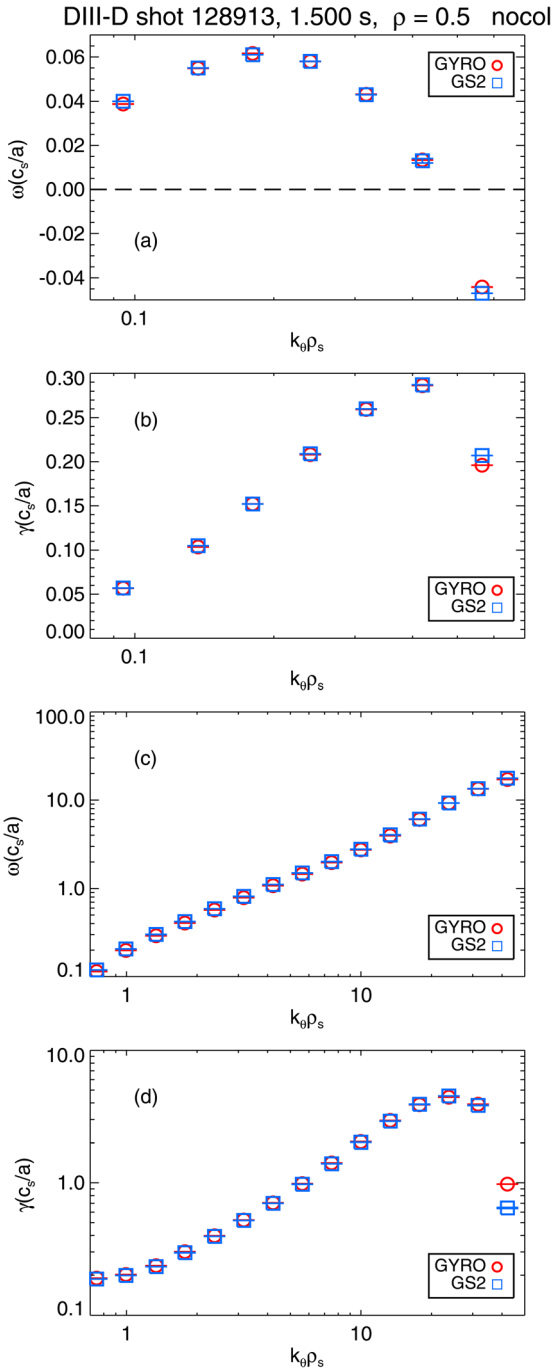

FIG. 2. (Color online) Same as Fig. 1 except omitting collisions and for $0.08 \leq k_\theta \rho_s \leq 0.7$ and $0.7 \leq k_\theta \rho_s \leq 50$.

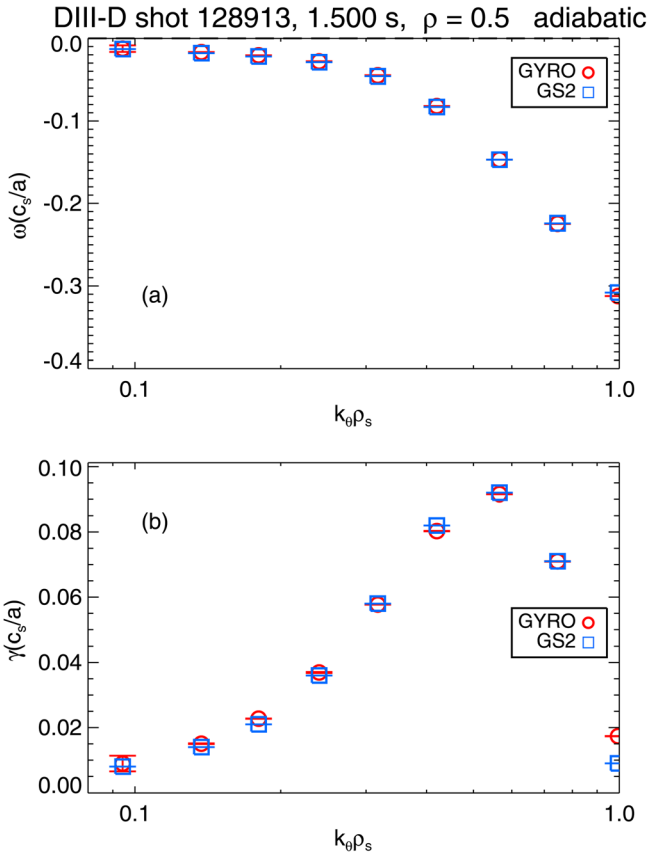

FIG. 3. (Color online) Same as Figs. 2(a) and 2(b) except for adiabatic electrons and $0.08 \leq k_\theta \rho_s \leq 1$.

Before presenting the fluxes, we first discuss uncertainties in the time-averages, which are not simply the time variations of the fluxes themselves. A method has been developed to calculate the uncertainties in the average fluxes based upon the statistics of subinterval averages.[39] However, it leads to very small error bars for stationary turbulence in simulations run for long times. In fact, the error bars vanish as run time increases. Consequently, the average fluxes from different codes would virtually never agree using this measure of uncertainty. A larger source of uncertainty in the time averages stems from the chaotic nature of a nonlinear simulation. The fluxes from "identical" simulations run for a finite time depend on initial conditions and even on the particular processors utilized. To our knowledge, there have been no systematic studies of these uncertainties to date. Although worthwhile, such studies would be very time-consuming and beyond the scope of this work.

In lieu of a rigorous quantification of the uncertainties in the average fluxes from a single simulation, we have formulated a heuristic metric for the agreement between fluxes from two simulations. For two functions of time f_1 and f_2, we define

$$\Delta \equiv \frac{|\langle f_1 \rangle - \langle f_2 \rangle|}{\max(\sigma_1, \sigma_2)}, \tag{1}$$

where the angled brackets denote time averages and σ_1 and σ_2 are the standard deviations of $f_1(t)$ and $f_2(t)$, respectively (*not* of $\langle f_1 \rangle$ and $\langle f_2 \rangle$). The expression is zero for perfect agreement and unity if the time average of either function lies within one standard deviation of the other function. Physically, the measure quantifies the difference in time-averaged fluxes relative to their inherent time variability represented by the standard deviations. We define adequate agreement as $\Delta < 1$, although this choice is somewhat arbitrary since, by the previous discussion, there is presently no pass/fail test.

Shown in Fig. 4 are time traces of the normalized (a) electron, (b) main ion (D), (c) impurity ion (C^{6+}) electrostatic energy fluxes, (d) electron energy flux from $\mathbf{B}_\perp$ fluctuations, and (e) electron, and (f) main ion electrostatic particle

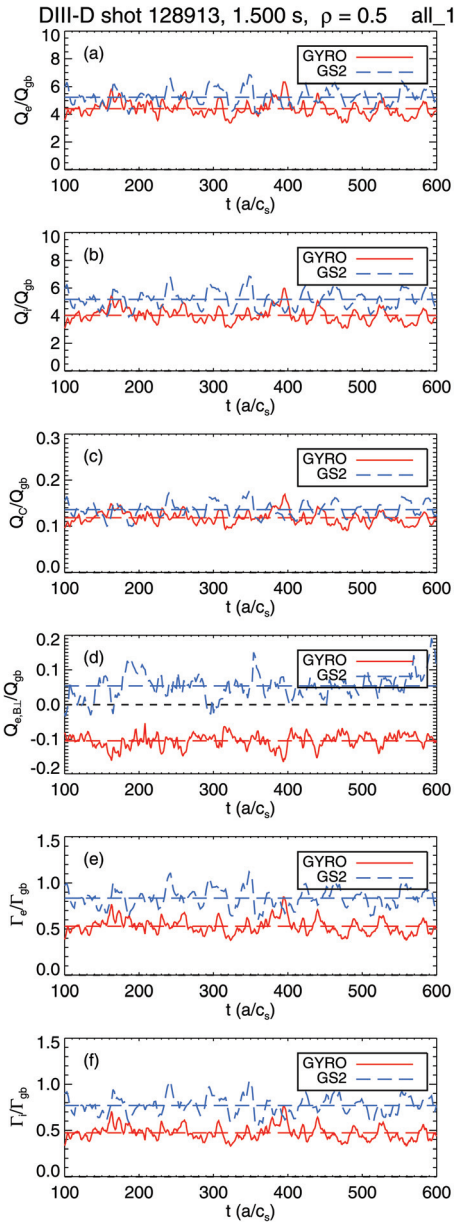

FIG. 4. (Color online) Gyro-Bohm-normalized (a) electron, (b) main ion (D), (c) impurity ion (C^{6+}) electrostatic energy fluxes, (d) electron energy flux from $\mathbf{B}_\perp$ fluctuations, and (e) electron, and (f) main ion electrostatic particle fluxes at $\rho = 0.5$ including collisions (corresponds to linear results of Fig. 1). Straight dashed lines indicate averages over the time range shown.

fluxes including collisions. (By charge conservation, the impurity flux Γ_C is simply $(\Gamma_e - \Gamma_i)/6$.) The time averages with standard deviations and the metric for code agreement Δ are listed in Table II. By the criterion $\Delta < 1$, none of the fluxes are strictly in agreement between codes, although the carbon energy flux only slightly fails the somewhat arbitrary criterion and the electromagnetic energy flux is very small. The disagreements in the other fluxes cannot be attributed to the slight differences in growth rates in the TEM region evident in Fig. 1(d). This is because the fluxes peak in the ITG range (where linear agreement is good), as shown in Fig. 5 for the electron energy flux spectra. Agreement between codes also extends to the shapes of the spectra themselves.

TABLE II. Normalized fluxes and measure of agreement for simulation with collisions.

	GYRO	GS2	Δ
Q_e/Q_{gB}	4.41 ± 0.54	5.24 ± 0.60	1.37
Q_i/Q_{gB}	4.03 ± 0.52	5.18 ± 0.64	1.80
Q_C/Q_{gB}	0.118 ± 0.014	0.136 ± 0.016	1.08
$Q_{B\perp}/Q_{gB}$	-0.104 ± 0.019	0.054 ± 0.0366	4.32
Γ_e/Γ_{gB}	0.530 ± 0.080	0.835 ± 0.102	2.98
Γ_i/Γ_{gB}	0.473 ± 0.075	0.770 ± 0.097	3.07

As was done for the linear calculations, we next omit collisions in the nonlinear simulations. The fluxes are shown in Fig. 6, and the averages and Δ are given in Table III. We see that all the fluxes agree between codes (again, by the criterion $\Delta < 1$). The normalized electron energy flux spectra are plotted in Fig. 7, where again, the codes agree well. In contrast to the collisional results, the GS2 spectrum is very slightly downshifted from the GYRO spectrum. We observe that the locations of the peaks of the spectra are approximately half those of the collisional spectra.

We also observe the magnitudes of all fluxes but the electromagnetic flux in the collisionless case is much greater than the corresponding collisional fluxes, which is consistent with the larger growth rates without collisions. This can explain some of the poorer agreement between the codes when including collisions: Except for the electron energy fluxes, the absolute differences between the GYRO and GS2 average fluxes are actually the same or smaller with collisions than without. Thus, almost none of the fluxes exhibit large absolute differences between the codes.

IV. SUMMARY

The applications of gyrokinetic microstability computations are becoming increasingly widespread. Consequently, verification and validation (V&V) of the codes and establishment of code benchmarks are necessary. Analysis or simulation by a particular code should be viewed skeptically until the code has met these benchmarks. The goal of this

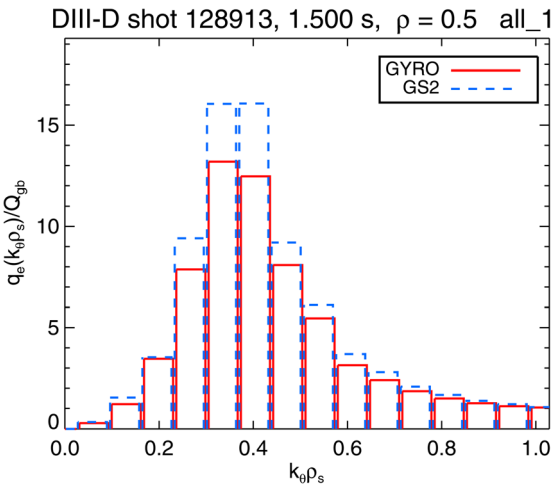

FIG. 5. (Color online) Normalized electron energy-flux spectra versus $k_\theta \rho_s$ at $\rho = 0.5$ including collisions [corresponds to time traces of Fig. 4(a)].

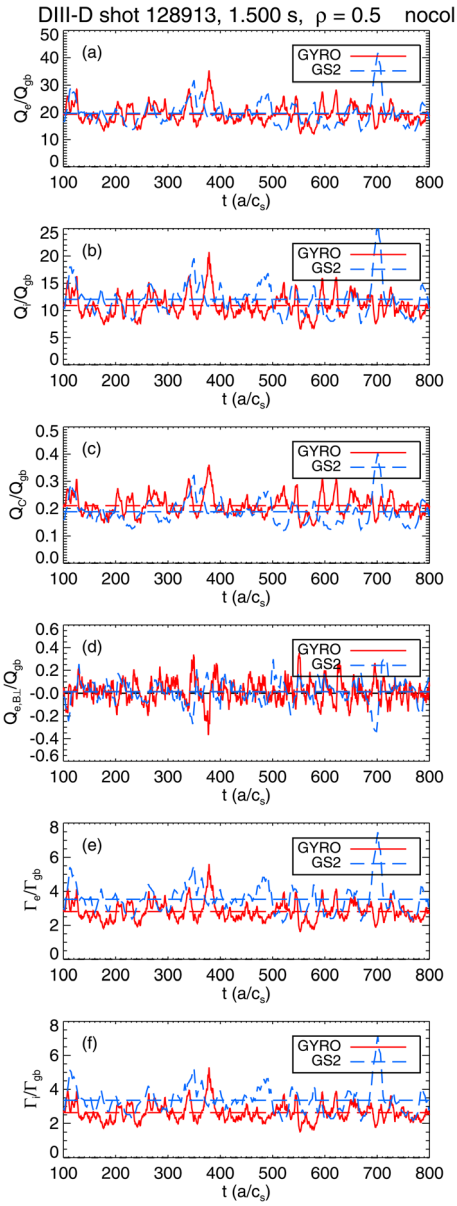

FIG. 6. (Color online) Same as Fig. 4 except omitting collisions (corresponds to linear results of Fig. 2).

continuing work—creation of experimentally relevant benchmarks for microstability codes—leads naturally to a more practical goal: verification and validation of nonlinear microstability codes.

We have presented comparisons between GYRO and GS2 of linear and nonlinear simulations for a particular discharge[13,17] at a particular time in the "confinement" region ($\rho = 0.5$) of the plasma. These simulations include electromagnetic fluctuations, passing and trapped electrons, plasma shaping (Miller formalism), electron collisions, and one impurity (C^{+6}). We have postponed inclusion of $\mathbf{E} \times \mathbf{B}$ flow shear for future work. Flux-tube geometry is valid for the nonlinear simulations since $\rho^* < 0.004$ (see Table I). We find excellent linear agreement between the codes with and without collisions except for the growth rates in the range $1.5 \leq k_\theta \rho_s \leq 4$ with collisions. Even that disagreement is less than 20% of the average of the GYRO and GS2 growth rates.

TABLE III. Normalized fluxes and measure of agreement for simulations without collisions.

	GYRO	GS2	Δ
Q_e/Q_{gB}	19.3 ± 3.4	19.7 ± 4.6	0.08
Q_i/Q_{gB}	10.9 ± 2.1	12.0 ± 2.9	0.39
Q_C/Q_{gB}	0.21 ± 0.04	0.19 ± 0.05	0.47
$Q_{B\perp}/Q_{gB}$	0.015 ± 0.096	0.013 ± 0.106	0.024
Γ_e/Γ_{gB}	2.81 ± 0.55	3.53 ± 0.82	0.88
Γ_i/Γ_{gB}	2.63 ± 0.51	3.36 ± 0.78	0.93

Because there is no established definition of the uncertainties in the fluxes from a nonlinear simulation, we have formulated a metric to judge agreement between the codes. We define adequate agreement when the time average of a flux from one code falls within one standard deviation of the flux from the other code. By this criterion, we find agreement of all fluxes between codes when neglecting collisions, but disagreement when collisions are included. We find that GS2 predicts fluxes that are larger (or more positive) than GYRO. Work to resolve this discrepancy is ongoing. Nevertheless, we have constructed linear and nonlinear benchmarks including transverse magnetic fluctuations, accurate plasma shape, three kinetic species, and electron collisions (linear benchmarks only) that can serve as tests of other codes.

V. FUTURE WORK

The obvious next step is to resolve the nonlinear disagreements between the codes when electron collisions are included. Beyond that, we will include equilibrium $\mathbf{E} \times \mathbf{B}$ flow shear. This capability exists in both GYRO and GS2. These comparisons would nicely dovetail into existing validation efforts that must include equilibrium flow shear when rotation is important[17,18] For example, the GS2 results with $\mathbf{E} \times \mathbf{B}$ flow shear could contribute to the GYRO/TGLF/GEM comparisons found in Ref. 40. Thereafter, comparisons at another radius, e.g., closer to the edge, should be made. Not only linear frequencies and nonlinear fluxes should be compared but also nonlinear fluctuation characteristics, which could contribute to validation efforts such as described in Refs. 18 and 20.

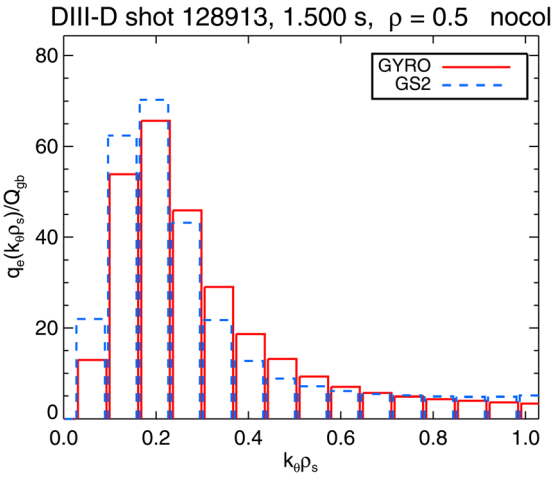

FIG. 7. (Color online) Same as Fig. 5 except omitting collisions [corresponds to time traces of Fig. 6(a)].

TABLE IV. Translations between non-identical GYRO and GS2 input profile parameters.

Parameter	GYRO	GS2
$s_\kappa = r\,\mathrm{dln}(\kappa)/\mathrm{d}r$	S_KAPPA	(*r*/kappa) kappri
δ	DELTA	sin(tri)
$s_\delta = r\,\mathrm{d}\delta/\mathrm{d}r$	S_DELTA	*r* cos(tri) tripri
β_e	BETAE_UNIT	$(B_0/B_{\mathrm{unit}})^2$ beta[a]
$\nu_{ei}\,a/c_s$	NU_EI	$2^{1/2}$ vnewk$_e$[a]

[a]for $m_{\mathrm{ref}} = m_i$, $n_{\mathrm{ref}} = n_e$, and $T_{\mathrm{ref}} = T_e$.

Code comparisons should utilize other discharges stressing different physics, e.g., high β when magnetic fluctuations are important, or extreme shaping. Ideally, this would be coordinated with ongoing validation efforts, e.g., Refs. 17–20 which heretofore have compared only one code (the "validation" code) to experiment. Since our data reader would most likely not be identical to that of the validation group, the first result would be a verification of the data readers. We would then perform the code verification procedure outlined earlier using profiles that give the best code agreement with experiment (some may have been adjusted by the validation group within experimental uncertainties). During the procedure, errors may be found in the validation code, requiring revisiting the validation exercise and perhaps further adjusting profiles within experimental uncertainties. If the profiles must be adjusted significantly to reach agreement with experiment, the verification effort would be repeated, leading to an iterative procedure. Such a coordinated effort would greatly enhance confidence in the validation results.

Another code should be introduced into the comparisons. Agreement among three codes would be much more convincing than agreement between two. Because GS2 is strictly a flux-tube code, all three codes would have to utilize periodic radial boundary conditions or ρ^* should be very small. Ideally, the third code would be a PIC code, which would serve to compare PIC vs. continuum algorithms.

ACKNOWLEDGMENTS

The authors would like to acknowledge helpful discussions with Walter Guttenfelder. This work was supported by the U.S. Department of Energy under Grants DE-FG02-08ER54978, DE-FG02-07ER54917, DE-FG02-06ER54871, and DE-FG02-95ER54309. The simulations were performed on the Franklin and Hopper systems at the National Energy Research Scientific Computing Center, which is supported by the U.S. Department of Energy under contract DE-AC02-05CH11231.

APPENDIX: DIFFERENCES BETWEEN GYRO AND GS2 NORMALIZATIONS AND INPUT PARAMETERS

- The GYRO reference density and temperature are those of the electrons and the reference mass and charge are those of the main ion, whereas the user may choose the references in GS2. Comparison between the codes is simplified if the user defines the GS2 references the same as GYRO.
- The GYRO reference velocity is the main ion sound speed $c_s \equiv (kT_e/m_i)^{1/2}$, whereas that in GS2 is $(2kT_{ref}/m_{ref})^{1/2}$. Again, comparison between the codes is simplified if the user defines the GS2 reference temperature and mass the same as GYRO.
- The GYRO reference magnetic field is $B_{\mathrm{unit}} \equiv B_0\,a^2(\rho/r)\,\mathrm{d}\rho/\mathrm{d}r$, where B_0, ρ, and r are defined in the first paragraph of Sec. III. The GS2 field is arbitrary but can be taken as B_0 for convenience. B_{unit} is typically significantly larger than B_0, e.g., a factor $\sim$1.4 larger for the plasma analyzed in this paper. This is important when comparing fluxes between the codes because they are normalized to the gyro-Bohm fluxes that scale as B^{-2}.
- In GS2, one specifies the dimensionless poloidal wave number aky $\equiv k_\theta \rho_{ref}$, whereas GYRO uses the toroidal mode number n $\equiv$ int[aky $r/(aq\rho^*_{\mathrm{unit}})$], where ρ^*_{unit} is defined using B_{unit} and we assume $\rho_{ref} = \rho_s$. In spite of the difference in the definitions of gyroradius, the product of wave number and gyroradius is the same for both codes, i.e., $k_{\theta,\mathrm{GYRO}} = k_{\theta,\mathrm{GS2}}\,(B_{\mathrm{unit}}/B_0)$.
- The real components of frequencies from linear GYRO simulations are positive for propagation in the electron direction. The opposite applies to GS2.
- Input plasma parameters that are defined differently and the relationships between them are given in Table IV.

[1]J. Candy and R. E. Waltz, J. Comput. Phys. **186**, 545 (2003).
[2]W. Dorland, F. Jenko, M. Kotschenreuther, and B. N. Rogers, Phys. Rev. Lett. **85**, 5579 (2000).
[3]Y. Chen and S. E. Parker, Phys. Plasmas **16**, 052305 (2009).
[4]A. M. Dimits, B. I. Cohen, W. M. Nevins, and D. E. Shumaker, Nucl. Fusion **41**, 1725 (2001).
[5]W. X. Wang, Z. Lin, W. M. Tang, W. W. Lee, S. Ethier, J. L. V. Lewandowski, G. Rewoldt, T. S. Hahm, and J. Manickam, Phys. Plasmas **13**, 092505 (2006).
[6]R. L. Miller, M. S. Chu, J. M. Greene, Y. R. Lin-Liu, and R. E. Waltz, Phys. Plasmas **5**, 973 (1998).
[7]J. Candy, Plasma Phys. Controlled Fusion **51**, 105009 (2009).
[8]See http://fusion.gat.com/theory/Efit for a history, description, and execution instructions.
[9]K. H. Burrell, Phys. Plasmas **4**, 1499 (1997).
[10]M. Shimada, D. J. Campbell, V. Mukhovatov, M. Fujiwara, N. Kirneva, K. Lackner, M. Nagami, V. D. Pustovitov, N. Uckan, J. Wesley, N. Asakura, A. E. Costley, A. J. H. Donné, E. J. Doyle, A. Fasoli, C. Gormezano, Y. Gribov, O. Gruber, T. C. Hender, W. Houlberg, S. Ide, Y. Kamada, A. Leonard, B. Lipschultz, A. Loarte, K. Miyamoto, V. Mukhovatov, T. H. Osborne, A. Polevoi, and A. C. C. Sips, Nucl. Fusion **47**, S1 (2007).
[11]J. Candy and R. E. Waltz, Phys. Rev. Lett. **91**, 045001 (2003).
[12]D. R. Ernst, P. T. Bonoli, P. J. Catto, W. Dorland, C. L. Fiore, R. S. Granetz, M. Greenwald, A. E. Hubbard, M. Porkolab, M. H. Redi, J. E. Rice, K. Zhurovich, and the Alcator C-Mod Group, Phys. Plasmas **11**, 2637 (2004).
[13]A. E. White, L. Schmitz, G. R. McKee, C. Holland, W. A. Peebles, T. A. Carter, M. W. Shafer, M. E. Austin, K. H. Burrell, J. Candy, J. C. DeBoo, E. J. Doyle, M. A. Makowski, R. Prater, T. L. Rhodes, G. M. Staebler, G. R. Tynan, R. E. Waltz, and G. Wang, Phys. Plasmas **15**, 056116 (2008).
[14]L. Lin, M. Porkolab, E. M. Edlund, J. C. Rost, C. L. Fiore, M. Greenwald, Y. Lin, D. R. Mikkelsen, N. Tsujii, and S. J. Wukitch, Phys. Plasmas **16**, 012502 (2009).
[15]A. Casati, T. Gerbaud, P. Hennequin, C. Bourdelle, J. Candy, F. Clairet, X. Garbet, V. Grandgirard, O. D. Gurcan, S. Heuraux, G. T. Hoang, C. Honoré, F. Imbeaux, R. Sabot, Y. Sarazin, L. Vermare, and R. E. Waltz, Phys. Rev. Lett. **102**, 165005 (2009).
[16]L. Lin, M. Porkolab, E. M. Edlund, J. C. Rost, M. Greenwald, N. Tsujii, J. Candy, R. E. Waltz, and D. R. Mikkelsen, Plasma Phys. Controlled Fusion **51**, 065006 (2009).
[17]C. Holland, A. E. White, G. R. McKee, M. W. Shafer, J. Candy, R. E. Waltz, L. Schmitz, and G. R. Tynan, Phys. Plasmas **16**, 052301 (2009).

[18]A. E. White, W. A. Peebles, T. L. Rhodes, C. H. Holland, G. Wang, L. Schmitz, T. A. Carter, J. C. Hillesheim, E. J. Doyle, L. Zeng, G. R. McKee, G. M. Staebler, R. E. Waltz, J. C. DeBoo, C. C. Petty, and K. H. Burrell, Phys. Plasmas **17**, 056103 (2010).
[19]J. C. DeBoo, C. Holland, T. L. Rhodes, L. Schmitz, G. Wang, A. E. White, M. E. Austin, E. J. Doyle, J. Hillesheim, W. A. Peebles, C. C. Petty, Z. Yan, and L. Zeng, Phys. Plasmas **17**, 056105 (2010).
[20]J. C. Rost, L. Lin, and M. Porkolab, Phys. Plasmas **17**, 062506 (2010).
[21]J. Candy, R. E. Waltz, S. E. Parker, and Y. Chen, Phys. Plasmas, **13**, 074501 (2006).
[22]S. E. Parker, W. Dorland, R. A. Santoro, M. A. Beer, Q. P. Liu, W. W. Lee, and G. W. Hammett, Phys. Plasmas **1**, 1461 (1994).
[23]A. M. Dimits, G. Bateman, M. A. Beer, B. I. Cohen, W. Dorland, G. W. Hammett, C. Kim, J. E. Kinsey, M. Kotschenreuther, A. H. Kritz, L. L. Lao, J. Mandrekas, W. M. Nevins, S. E. Parker, A. J. Redd, D. E. Schumaker, R. Sydora, and J. Weiland, Phys. Plasmas **7**, 969 (2000).
[24]See https://fusion.gat.com/theory/CSPM for the goals and makeup of the Center.
[25]See http://w3.pppl.gov/theory/bin/PSACI-PAC04-Lee.pdf for the mission, makeup, and accomplishments of the Center.
[26]T. Trucano and D. Post, Guest Editors, Comput. Sci. Eng. **14**, 8 (2004).
[27]R. C. Davidson, Phys. Plasmas **14**, 050401 (2007).
[28]See http://www.pppl.gov/fsp/FSP_Summary_FILES/FSP_Program_Execution_Plan.pdf for "Fusion Simulation Program Execution Plan," September 2011.
[29]W. M. Nevins, G. W. Hammett, A. M. Dimits, W. Dorland, and D. E. Shumaker, Phys. Plasmas **12**, 122305 (2005).
[30]Y. Chen and S. E. Parker, Phys. Plasmas **14**, 082301 (2007).
[31]J. Candy and R. E. Waltz, Phys. Plasmas **13**, 032310 (2006).
[32]M. Kotschenreuther, G. Rewoldt, and W. M. Tang, Comput. Phys. Commun. **88**, 128 (1995).
[33]M. Barnes, W. Dorland, and T. Tatsuno, Phys. Plasmas **17**, 032106 (2010).
[34]I. G. Abel, M. Barnes, S. C. Cowley, W. Dorland, and A. A. Schekochihim, Phys. Plasmas **15**, 122509 (2008).
[35]M. Barnes, I. G. Abel, W. Dorland, D. R. Ernst, G. W. Hammett, P. Ricci, B. N. Rogers, A. A. Schekochihin, and T. Tatsuno, Phys. Plasmas **16**, 072107 (2009).
[36]See http://fusion.gat.com/THEORY/onetwo/ for a description of the code and execution instructions.
[37]See http://w3.pppl.gov/transp/ for a description of the code and execution instructions.
[38]J. Candy, private communication (2003).
[39]D. R. Mikkelsen, private communication (2011); W. M. Nevins, private communication (2008).
[40]T. L. Rhodes, C. Holland, S. P. Smith, A. E. White, K. H. Burrell, J. Candy, J. C. DeBoo, E. J. Doyle, J. C. Hillesheim, J. E. Kinsey, G. R. McKee, D. Mikkelsen, W. A. Peebles, C. C. Petty, R. Prater, S. Parker, Y. Chen, L. Schmitz, G. M. Staebler, R. E. Waltz, G. Wang, Z. Yan, and L. Zeng, Nucl. Fusion **51**, 063022 (2011).